TURBULENCE ANALYSIS OF A RECTANGULAR SEDIMENTATION BASIN USING NUMERICAL SIMULATION

Luísa Vieira Lucchese, luisa.lucchese@ufrgs.br
Edith Beatriz Camaño Schettini, bcamano@iph.ufrgs.br
Núcleo de Estudos em Transição e Turbulência, at Instituto de Pesquisas Hidráulicas - Universidade Federal do Rio Grande do Sul. Av. Bento Gonçalves, 9500. Porto Alegre, Brazil.

Abstract. *Rectangular sedimentation basins are used on drinking water treatment in the stage of water clarification. When used, they tend to be the major part of the water treatment facility. In order to analyze the turbulent instabilities that can occur, a Direct Numerical Simulation was performed. The Incompact3d code has been used to implement the boundary conditions, which uses sixth-order compact finite-difference schemes for the spatial scheme, and second-order Adams-Bashfort scheme for the time advancement. All of the variables are dimensionless. A comparative for the Stokes Law has been made, concerning monodisperse simulations. For the polydisperse simulations, the grain size curve has been discretized in 13 ranges of particles, and Stokes Law and Julien-Winterwerp model were implemented. The Reynolds Number based on the channel height were 10^4 and $2 \cdot 10^4$. In the initial times of the simulation, close to the left border, the Rayleigh-Taylor instability occurs. When the fluid that carries sediments touches the bottom of the tank, a turbidity current is formed. In this density current, one can observe Kelvin-Helmholtz occurring in the mixing layer. In some simulations, in advanced times, the hyperpycnal currents rise, becoming hypopycnal, due do the deposit of larger particles. One can observe small particle diameters can leave the tank with ease due to turbulence.*

Keywords: *sedimentation basin, turbulence, diffusion, numerical simulation*

1. INTRODUCTION

Drinking water treatment facilities consist of two complementary stages: clarification, that removes the solids suspended, and disinfection, that removes pathogens [7]. The clarification stage starts with the water pumping to the site, followed by coagulation (usually made with aluminum sulfate), flocculation and then, sedimentation. For the sedimentation, circular, rectangular, or even square tanks can be used. In the present work, the authors analyze rectangular sedimentation basins, which require no electricity, but a lot of space. A rectangular sedimentation tank is also less susceptible to hydraulic short-circuiting and the effects of gravity currents. Gravity currents are a known phenomenon that can happen in sedimentation basins [5]. They occur when a denser fluid flows under a lighter one, and can be triggered by temperature and solid concentration.

Traditional models on sedimentation on these basins consider there is no turbulence occurring on the tanks, so there is a laminar flow. If the flow was completely laminar, the particle would sediment in a constant rate, dictated by the Stokes Law [5]. And so, rectangular sedimentation basins have been designed worldwide [1] [5] following this rule, making the length of the tank enough so that a particular diameter particle can deposit, even if it has entered the tank in the upper margin. Although, since the dimensions of the tank can be particularly large (dozens of meters), the laminar flow assumption may not be completely right, and that is one thing that the present paper intends to show.

Previous research was conducted by Goula et al. (2008) [10] and Al-Sammarraee et al. (2009) [2], both using the Fluent code. Goula et al. (2008) [10] performed the simulation with the $k-\omega$ turbulence model on RANS, while Al-Sammarraee et al. (2009) [2] used the $k-\epsilon$ turbulence model on RANS, and performed simulations on LES methodology too. According to research of Goula et al. (2008), most of the deposit occurs on the start or center of the tank [10]. Goula et al. (2008) did not observe a density current on their simulations, but acknowledged that they may occur in real tanks [10]. Al-Sammarraee et al. (2009) [2] observed that the effluent of the tank held bigger fractions of smaller particles, showing that these particles have more difficulty on depositing. Zhang (2014) [15] also performed research in this field, but his aim was more technical and oriented to teach the reader to perform simulations of sedimentation tanks on the Fluent code. Most of his simulations used the RANS $k-\epsilon$ model.

Not only the present paper shows that it is a turbulent flow, it also has turbulent instabilities. Analyzed instabilities include Kelvin-Helmholtz, Rayleigh-Taylor and the formation of turbidity currents and plumes.

Another different approach was given in the research of the present authors: a rather different sedimentation model for the particles has been implemented in the used code, the Julien-Winterwerp model, proposed by Julien (2010) [11] based on the model of Winterwerp (1999) [14]. This model was compared to the traditional Stokes model. The Stokes model is one of the most applied models when it comes to particle settling. It considers all particles as spherical with constant density, and with constant drag coefficients, what, as suggested Edzwald (2011)[8], is just an approximation. To best search flocculation and sedimentation effects, some literature [4] [7] [6] separates the sedimentation in four types: discrete settling (Type I), flocculant settling (Type II), hindered settling (Type III), and compressive settling (Type IV). Stokes' Law is a good approximation when the sedimentation is Type I, which means, when the particles do not flocculate. The sedimen-

tation types I and II are more similar to what happens in the sedimentation tanks, depending on properties of the settling basin inflow [7] .
The main objective of the present paper is to observe turbulent instabilities concerning a sedimentation basin-like setting for the simulated tank.

2. METHODOLOGY

The *Incompact3d* code [12], used in the present study, uses dimensionless variables. The Reynolds Number used for the present work is the global Reynolds Number for the flow in the tank:

$$Re = \frac{u_0 h}{\nu}. \tag{1}$$

In Eq. 1, u_0 is the horizontal velocity in the affluent, $h = L_y/2$ is the size of the tank inlet and ν is the kinematic viscosity of the fluid. In $\vec{u} =< u_x, u_y >$ the two velocity components are defined.
The Schmidt number $Sc = \nu/k$ is the ratio between kinematic viscosity ν and molecular diffusivity k. The solids concentration on the fluid is:

$$\Phi = \frac{\rho - \rho_{min}}{\rho_{max} - \rho_{min}}, \tag{2}$$

in which ρ_{min} is the density in pure water, ρ_{max} is the density of water plus sediment, and ρ is the density in a mesh node. Therefore, Φ always varies between 0 and 1, independently of fluids involved. In polidisperse cases, which means, for the description of a granulometric curve, the proportion of each discretized range is maintained from the original curve, and their mass fractions summed result 1.

Although by the Eq. 2 there can be any densities, the difference between densities should be small because the Boussinesq approximation is used. The Boussinesq approximation considers the rate of change in the volume is constant ($\Delta\rho/\rho << 1$). Since the flocks are on low concentration and the fluid is considered incompressible, the Boussinesq approximation is valid.
The simulations have used the Equations of Continuity, Navier-Stokes, and Transport-Diffusion:

$$\vec{\nabla} \cdot \vec{u} = 0, \tag{3}$$

$$\frac{\partial \vec{u}}{\partial t} + (\vec{u} \cdot \nabla)\vec{u} = -\nabla p + \Phi \vec{e}_g + \frac{1}{Re}\nabla^2 \vec{u}, \tag{4}$$

$$\frac{\partial \Phi}{\partial t} + (\vec{u} + u_s \vec{e}_g) \cdot \nabla \Phi = \frac{1}{ReSc}\nabla^2 \Phi. \tag{5}$$

In the equations 3, 4 and 5, $\vec{e}_g$ is a versor in the $-\hat{j}$ direction, $\vec{u}$ is the velocity vector, t is the time, and p the pressure.
The water plus sediment inlet in the field was localized in the upper left boundary on the computational domain. In Fig. 1 the schema of the simulated tank can be observed. u_0 is the inlet velocity, Φ is the inlet concentration (in this case, $\Phi = 1$).

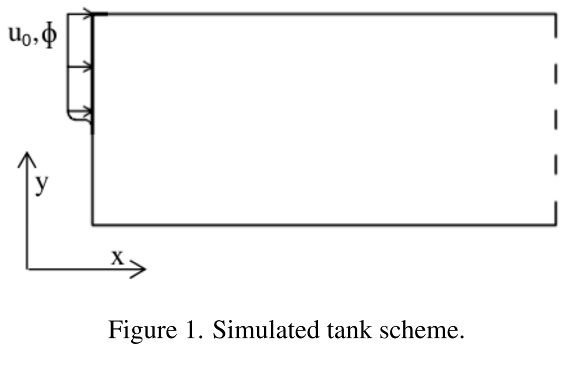

Figure 1. Simulated tank scheme.

The base code for the Numerical Simulations is *Incompact3d (http://www.incompact3d.com)* [12]. The code has been edited in Fortran-90. The turbulence has been acquired without the implementation of any turbulence model. This code has been used in fluid mechanics simulations for different types of flows.
The computational mesh is cartesian and structured, with constant mesh refinement. The boundary conditions are explicit

in Fig. 2. Free-slip ($\partial u_x/\partial y = 0$ and $u_y = 0$) boundary conditions have been implemented in the surface ($y = L_y$) and bottom ($y = 0$) boundaries, while no-slip was implemented in $x = 0$ and $0 \leq y < L_y/2$. The inlet of velocity and sediments are implemented in $x = 0$ and $L_y/2 \leq y < L_y$. The outlet is localized on $x = L_x$, and the Robin equation has been used, in which c is a convective velocity. The Robin condition has been used because the characteristics of the sediment beyond the limits of the computational field are unknown, and letting this sediment back inside the tank could bring wrong sediment characteristics to the simulation. The equation for the outlet is:

$$\frac{\partial \vec{u}}{\partial t} + c\frac{\partial \vec{u}}{\partial x} = \vec{0}. \tag{6}$$

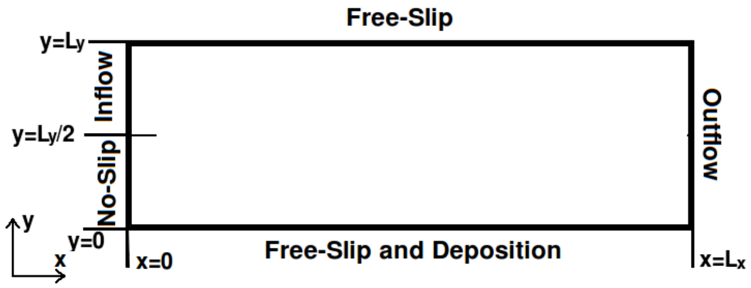

Figure 2. Boundary conditions for the tank.

For the inlet, both of the velocity and concentration, a hyperbolic tangent-like equation was adopted:

$$\vec{u}(y) = \frac{1}{2}\left(tanh\left(y - \frac{L_y}{2}\right) + 1\right)\hat{i}. \tag{7}$$

This was chosen because sudden changes on the velocity and concentration field can lead to great vorticity and numerical instability.

The *Incompact3d* code uses sixth-order compact finite-difference schemes [13]. For temporal scheme a second-order Adams-Bashfort method has been used. The vectorial variables are defined in the mesh node, while the scalar ones are defined in the center of each mesh, representing the area defined by four mesh nodes.

3. RESULTS

The performed simulations are monodisperse (one particle size) or polidisperse (13 classes of particle size). The monodisperse were used for comparation with the Stokes Model. The polidisperse classes of particle size were based on Goula et al. (2008) [10], shown in Tab. 1. This table also shows the settling velocities for the Stokes' and Julien-Winterwerp's models. For particle diameters smaller than $336\mu m$, Julien-Winterwerp's model produces higher settling velocities, and for bigger diameters, the relation inverts itself.

A comparison between the Stokes Law and what have occurred in simulated tanks have been made. For this comparison, there was used only one particle size (monodisperse), as the theory of discrete settling (Type I), wherein the Stokes Law applies, assumes that all particles are spherical and the particle size distribution is uniform. In Fig. 3, the comparison can be seen. The red bar indicates the distance that a particle which enters the tank near the surface runs horizontally before depositing, according to Stokes law. This parameter is widely used for the design of settling tanks [3] [5]. For $Re = 10^4$ (Fig. 3a and 4a), $x_{stokes} = 1.16$, and for $Re = 2 \cdot 10^4$ (Fig. 3b and 4b), $x_{stokes} = 2.32$. One can observe the maximum theoretical deposition distance, based on Stokes Law, approaches the maximum deposition distance occurring in the simulated settling tanks. For accumulated deposit, the scenario remains the same. One can see in Fig. 4 the deposit occurs mainly in the left of the tank, and respects the Stokes model limits given. Mass units, placed in ordinate, are the sum of the depositing particles concentration. One may observe each time step (Δt), $\Phi \cdot N_y/2 \approx 50$ mass unities enter the computational field.

For the tank itself, in order to estimate correctly the leading parameters, some assumptions were made. The entry velocity for the Brazilian standard varies between 0.5 and $1cm/s$ [1]. The particle density was considered $1.03g/cm^3$ [4]. The depth of the water in the tanks varies from 3 to $5m$ [7], and the considered depth was $4m$, so that $h = 2m$ is the inlet size for the simulations. The calculated Reynolds numbers for $\tilde{u}_x = 0.005m/s$ and $\tilde{u}_x = 0.010m/s$ (the tilde indicates dimensional quantities) are, respectively, $Re = 10^4$ and $Re = 2 \cdot 10^4$. To transform the particle's settling velocities into dimensionless quantities, the dimensional velocities were divided by u_0, and are presented in Tab. 2 .

Table 1. Definition of the particle classes and settling velocities.

Class	Medium Diameter (μm)	Mass Fraction [10]	u_s Stokes (m/s)		u_s Julien-Winterwerp (m/s)
1	20	0.025	6.905E-06	<	2.828E-05
2	50	0.027	4.315E-05	<	1.118E-04
3	80	0.039	1.105E-04	<	2.263E-04
4	120	0.066	2.486E-04	<	4.157E-04
5	170	0.095	4.989E-04	<	7.009E-04
6	200	0.114	6.905E-04	<	8.944E-04
7	250	0.125	1.079E-03	<	1.250E-03
8	350	0.123	2.115E-03	>	2.071E-03
9	450	0.112	3.495E-03	>	3.019E-03
10	550	0.100	5.222E-03	>	4.079E-03
11	650	0.077	7.293E-03	>	5.240E-03
12	750	0.057	9.710E-03	>	6.495E-03
13	850	0.040	1.247E-02	>	7.837E-03

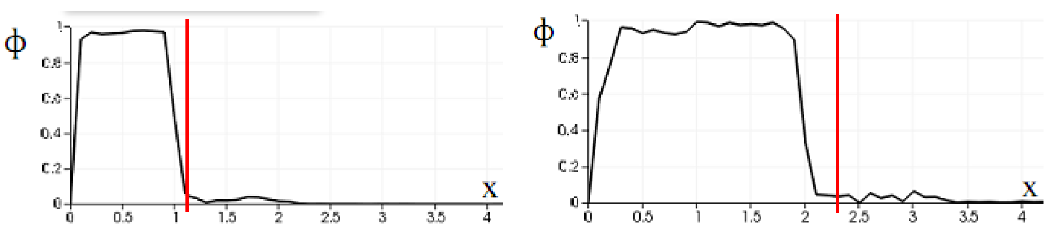

(a) (b)

Figure 3. Instantaneous deposition on $t = 12$ (in black) and Stokes model prediction for deposition range (in red). (a) $Re = 10^4$, $u_s = 4.315 \cdot 10^{-3} m/s$. (b) $Re = 2 \cdot 10^4$, $u_s = 4.315 \cdot 10^{-3} m/s$.

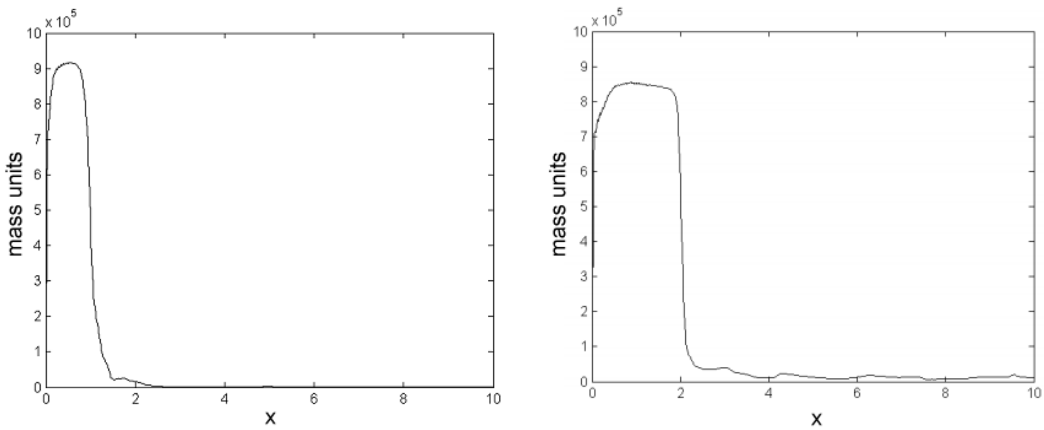

(a) (b)

Figure 4. Accumulated deposit on $t = 20$. (a) $Re = 10^4$, $u_s = 4.315 \cdot 10^{-3} m/s$. (b) $Re = 2 \cdot 10^4$, $u_s = 4.315 \cdot 10^{-3} m/s$.

The simulations performed had $L_y = 2$, and the horizontal length varied from $L_x = 10$ to $L_x = 30$. The vertical mesh was always $N_y = 201$, while the horizontal mesh varied from $N_x = 1001$ to $N_x = 3001$ with the length, so that the space meshes are approximately square, with $\Delta x = \Delta y = 0.01$. The temporal step used for most simulations is $\Delta t = 2 \cdot 10^{-5}$.

The first shown simulation, on Figs. 5 and 6, has $L_x = 10$, $Re = 10^4$ and uses the model of Stokes. In the time $t = 3$, for Class 6, it is possible to see the Rayleigh-Taylor instability in the tank inlet. For higher particle classes, at this point, deposition was already occurring. As the time advances, a density current is formed and a buoyant plume is formed near the surface of the tank. This plume leaves the tank without settling. Similar beahviour was observed for different

Table 2. Particle classes and dimensionless settling velocities.

Class	u_s for $Re = 10^4$ Stokes	u_s for $Re = 10^4$ Julien-Winterwerp	u_s for $Re = 2 \cdot 10^4$ Stokes	u_s for $Re = 2 \cdot 10^4$ Julien-Winterwerp
1	0.0014	0.0057	0.0007	0.0028
2	0.0086	0.0224	0.0043	0.0112
3	0.0221	0.0453	0.0110	0.0226
4	0.0497	0.0831	0.0249	0.0416
5	0.0998	0.1402	0.0499	0.0701
6	0.1381	0.1789	0.0690	0.0894
7	0.2158	0.2500	0.1079	0.1250
8	0.4229	0.4141	0.2115	0.2071
9	0.6991	0.6037	0.3495	0.3019
10	1.0443	0.8158	0.5222	0.4079
11	1.4586	1.0481	0.7293	0.5240
12	1.9419	1.2990	0.9710	0.6495
13	2.4943	1.5673	1.2471	0.7837

Reynolds Numbers and also for the Julien-Winterwerp model. The slight difference is that, for higher Reynolds numbers, the turbulent scales are richer. In Fig. 6, one can observe that ouflow starts letting solids out on $t \approx 6$. The smaller particles tend to leave more the tank. To ratify this statement, Fig. 6 also shows the division of the outlet concentration for the original concentration for each particle, which is given on Tab. 1. This graph shows that smaller particles have a greater chance of leaving the tank. The changes made on other simulations, regarding Reynolds Number and model of settling did not change this aspect. Yet, for Julien-Winterwerp model, the maximum sediment outflow slightly increased.

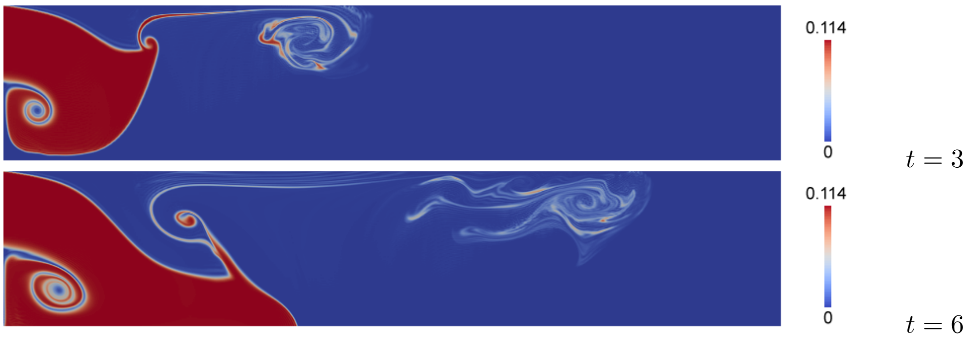

Figure 5. Concentration field on $t = 3$ and $t = 6$ for class 6 particles, for a simulation with $L_x = 10$, $Re = 10^4$ and using the Stokes' model.

Longer tanks, such as shown in Figs. 7, 8, 9 and 10 were simulated so one could observe what happens on advanced times, in the tank. This simulation was performed with $L_x = 30$, $N_x = 3001$, Stokes' model, and $Re = 2 \cdot 10^4$. In Figs. 7 and 8 it is possible to see the same kind of simulation start, with the formation of a Rayleigh-Taylor instability, and the subsequent formation of a turbidity current alongside the bottom of the tank. This turbidity current generates a mixing layer above itself, and in this mixing layer, one can see the Kelvin-Helmholtz instabilities occurring. Advancing in time, there is Fig. 9 showing the advance of the gravity current (for the smaller particles). Advancing more, on Fig. 10, with the deposition of the bigger particles, the current does not longer sustain itself as a hyperpycnal gravity current, and rises to the surface as a hypopycnal buoyant plume. This behaviour had already been observed in the experimental work of Ferreira (2013) [9]. As one can observe in the figures for this simulation, for bigger particles, there are no gravity currents, buoyant plumes, and for the biggest diameters, there is not even a Rayleigh-Taylor instability in the inlet, and the particles deposit straight ahead. Similar behaviour occurred for lower Re and for Julien-Winterwerp's model.

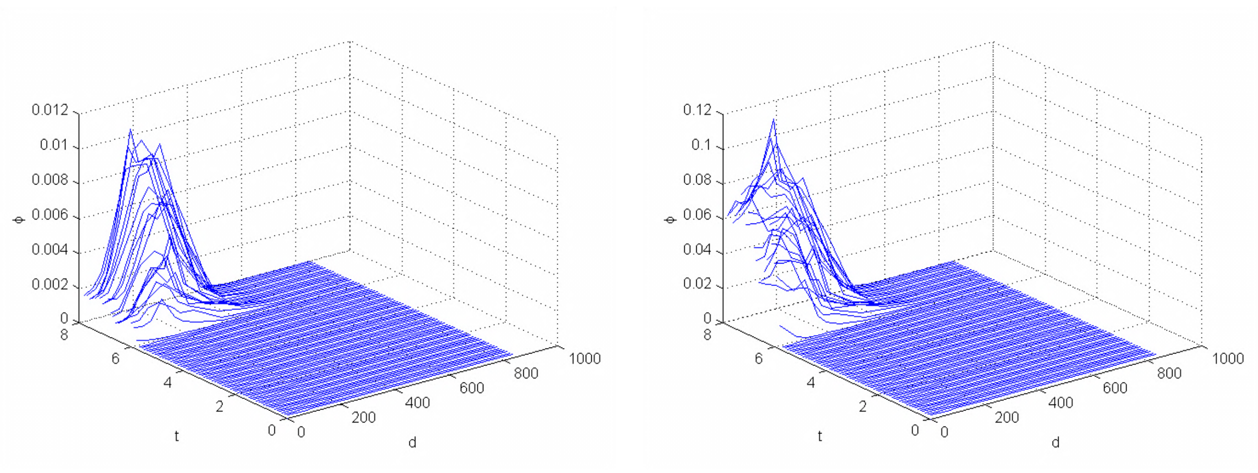

(a) (b)

Figure 6. (a) Outlet granulometric curves along time, for $L_x = 10$, $Re = 10^4$ and Stokes model. (b) Ratio between outlet and inlet granulometric curves along time, for the same simulation.

Figure 7. Concentration fields on $t = 4$ for particle classes 1, 5 and 11. Simulation with $L_x = 30$, $Re = 2 \cdot 10^4$ and Stokes' model.

Figure 8. Concentration fields on $t = 8$ for particle classes 1, 5 and 11. Simulation with $L_x = 30$, $Re = 2 \cdot 10^4$ and Stokes' model.

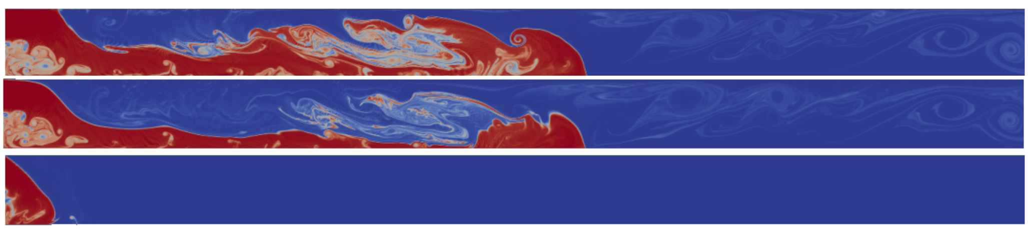

Figure 9. Concentration fields on $t = 20$ for particle classes 1, 5 and 11. Simulation with $L_x = 30$, $Re = 2 \cdot 10^4$ and Stokes' model.

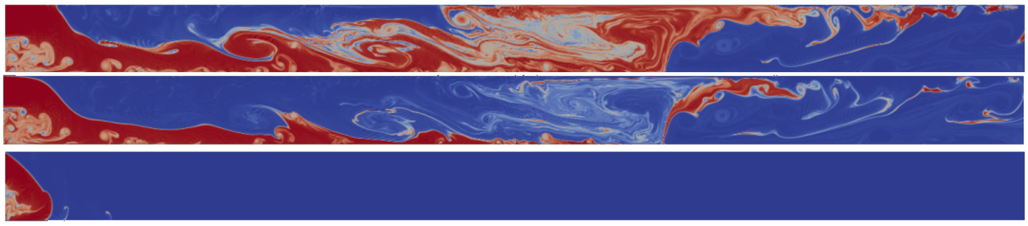

Figure 10. Concentration fields on $t = 30$ for particle classes 1, 5 and 11. Simulation with $L_x = 30$, $Re = 2 \cdot 10^4$ and Stokes' model.

4. CONCLUSIONS

Even though this is a limited analysis, mostly because it is 2-D, it was the first work to not implement turbulence models on the study of turbulence involved in settling on sedimentation basins. This work focused specifically on the observation of turbulence and turbulent instabilities. It was well-known that these instabilities occurred, but they had never been seen on computational simulations on a scientific approach.
The change of behaviour in the gravity current generated by the affluent, from hyperpycnal to hypopycnal, is an observed phenomena that also happens in experimental gravity currents. The present work shows that it can happen in sedimentation basins due to the deposit of the larger particles contained in the water with sediments. If this happens in a functioning sedimentation basin, it can bring harm to the effluent of the basin, because usually the water outlet is a channel in the tank surface.

5. ACKNOWLEDGEMENTS

The authors thank CNPq for the master's scholarship given to the first author.

6. REFERENCES

ABNT, 1992. "NBR 12216: projeto de estação de tratamento de água para abastecimento público". Rio de Janeiro, Brasil.
Al-Sammarraee, M.; Chan, A.; Salim, S. M.; Mahabaleswar, U. S, 2009. "Large-eddy simulations of particle sedimentation in a longitudinal sedimentation basin of a water treatment plant. Part I: particle settling performance." Chemical Engineering Journal, Vol.152, [n. 2-3], pp. 307-314.
ASCE, 1969. "Water Treatment Plant Design." American Water Works Association, New York.
Barroso, M. M., 2007. "Influência das micro e macropropriedades dos lodos de estações de tratamento de águas no desaguamento por leito de drenagem." Thesis. Escola de Engenharia de São Carlos, Universidade de São Paulo, São Carlos, Brasil.
Baruth, E. E. (Editor), 2005. "Water Treatment Plant Design". 4th ed., Ed. McGraw-Hill, New York, USA.
Cho, S. H.; Colin, F.; Sardin, M.; Prost, C., 1993. "Settling velocity model of activated sludge." Water Research, Vol. 27, n. 7, pp. 1237-1242.
Crittenden J. C.; Trussel, R. R.; Hand, D. W.; Howe, K. J.; Tchobanoglous, G., 2012. "Water Treatment Principles and Design." 3rd. Ed. MHW, Hoboken, USA.
Edzwald, J. K. (Ed.), 2011. "Water Quality and Treatment: a handbook on drinking water." 6th. ed. McGraw Hill, Denver, USA.
Ferreira, P. L. C., 2013. "Análise Comparativa entre Correntes de Densidade e Jatos". Master's thesis. Departamento de Hidromecânica e Hidrologia, Universidade Federal do Rio Grande do Sul, Porto Alegre.
Goula A. M.; Kostoglou, M.; Karapantsios, T. D.; Zouboulis, A. I., 2008. "CFD methodology for the design of sedimentation tanks in potable water treatment case study: the influence of a feed flow control baffle." Chemical Engineering Journal, Vol. 140, [n. 1-3], pp. 110-121.
Julien, P. Y., 2010. "Erosion and Sedimentation." 2nd. ed. Cambridge University Press, Cambridge, England.
Laizet, S.; Lamballais, E., 2009. "High-order compact schemes for incompressible flows: A simple and efficient method with quasi-spectral accuracy." Journal of Computational Physics, Vol. 228, pp. 5989-6015.
Lele, S., 1992. "Compact finite difference schemes with spectral-like resolution." Journal of Computational Physics, Vol.103, pp.16-42.
Winterwerp, J. C., 1999. "On the dynamics of high-concentrated mud suspensions." Delft: Delft University of Technology, Communications on Hydraulic and Geotechnical Engineering, n. 99-3.

Zhang, D., 2014. "Optimize sedimentation tank and lab flocculation unit by CFD". Master's thesis. Department of mathematical science and technology, Norwegian University of Life Sciences, Ås.

7. RESPONSIBILITY NOTICE

The author(s) is (are) the only responsible for the printed material included in this paper.